© 2020. Published by The Company of Biologists Ltd | Development (2020) 147, dev184895. doi:10.1242/dev.184895

STEM CELLS AND REGENERATION

RESEARCH ARTICLE

The atypical histone variant H3.15 promotes callus formation in *Arabidopsis thaliana*

An Yan[1], Michael Borg[2], Frédéric Berger[2] and Zhong Chen[1,*]

ABSTRACT

Plants are capable of regenerating new organs after mechanical injury. The regeneration process involves genome-wide reprogramming of transcription, which usually requires dynamic changes in the chromatin landscape. We show that the histone 3 variant HISTONE THREE RELATED 15 (H3.15) plays an important role in cell fate reprogramming during plant regeneration in *Arabidopsis*. H3.15 expression is rapidly induced upon wounding. Ectopic overexpression of H3.15 promotes cell proliferation to form a larger callus at the wound site, whereas *htr15* mutation compromises callus formation. H3.15 is distinguished from other *Arabidopsis* histones by the absence of the lysine residue 27 that is trimethylated by the POLYCOMB REPRESSIVE COMPLEX 2 (PRC2) in constitutively expressed H3 variants. Overexpression of H3.15 promotes the removal of the transcriptional repressive mark H3K27me3 from chromatin, which results in transcriptional de-repression of downstream genes, such as *WUSCHEL RELATED HOMEOBOX 11* (*WOX11*). Our results reveal a new mechanism for a release from PRC2-mediated gene repression through H3.15 deposition into chromatin, which is involved in reprogramming cell fate to produce pluripotent callus cells.

KEY WORDS: Callus formation, H3.15, Regeneration, H3K27me3, Cell fate reprogramming

INTRODUCTION

Plants have a remarkable regenerative capability to heal after injury by regenerating new tissue at sites of wounding. Under appropriate culture conditions, plants can regenerate entire individuals from a piece of tissue or even a single cell (Sugimoto et al., 2011). Wound-induced regeneration is usually initiated with the formation of a proliferating mass of pluripotent cells, termed callus. A callus contains a population of undifferentiated cells with proliferation potential, which are able to re-enter the cell cycle and continue to differentiate into new organs (Ikeuchi et al., 2013). Callus formation can be induced experimentally by wounding or in cell culture on callus-inducing medium (CIM) (Lee and Seo, 2018). Wound-induced callus formation involves the reprogramming of differentiated somatic cells to reacquire totipotency through cell dedifferentiation. This results from the action of transcription factors from the APETALA 2/ETHYLENE RESPONSE FACTOR (AP2/ERF) family, including WOUND INDUCED DEDIFFERENTIATION 1 (WIND1), WIND2, WIND3, WIND4 and ENHANCER OF SHOOT REGENERATION 1 (ESR1) (Iwase et al., 2011, 2017). WIND1 promotes wound-induced cell dedifferentiation through the activation of B-Type ARABIDOPSIS RESPONSE REGULATOR (ARR)-dependent cytokinin signaling (Iwase et al., 2011). Auxin-rich CIM-induced callus formation is commonly used as the first step in *de novo* organogenesis, followed by the incubation of callus on auxin-rich root-inducing medium (RIM) or cytokinin-rich shoot-inducing medium (SIM) to regenerate roots or shoots (Skoog and Miller, 1957). CIM-induced callus formation is initiated from pericycle cells of root explants and pericycle-like cells of aerial organs (Sugimoto et al., 2010). It has been proposed that CIM-induced callus formation resembles lateral root development, regardless of what types of tissue are used as explants (Atta et al., 2009; Sugimoto et al., 2010; Lee and Seo, 2018).

During callus formation, widespread changes in gene expression are required to reprogram the transcriptional state of somatic cells. Such genome-wide changes in transcription coincide with changes in chromatin modifications, including DNA methylation, post-translational modification of histones and exchange of histone variants (Ikeuchi et al., 2015b; Lee and Seo, 2018). The repressive modification H3K27me3 silences leaf-regulatory genes and is essential for leaf-to-callus transition in *Arabidopsis* (He et al., 2012), and for the prevention of unscheduled reprogramming of differentiated somatic cells (Ikeuchi et al., 2015a). These contrasting roles indicate that dynamic changes in H3K27me3 are probably required for reprogramming during regeneration. The regulation of dynamic changes in chromatin depends on the activities of histone H3 variants (Malik and Henikoff, 2003; Henikoff et al., 2004; Weber and Henikoff, 2014). In multicellular eukaryotes, the histone H3 family comprises three major types of variants: canonical H3.1 and H3.3 variants, and the centromeric variant CenH3 (Malik and Henikoff, 2003; Loyola and Almouzni, 2007; Jiang and Berger, 2017b). In *Arabidopsis*, H3.1 is essential for the maintenance of H3K27me3 through cell division (Jiang and Berger, 2017a). H3.1 deposition relies on the activity of the Chromatin Assembly Factor 1 (CAF-1) complex (Kaya et al., 2000; Jiang and Berger, 2017a), whereas H3.3 deposition is primarily mediated by a complex containing the chaperone HIRA (Nie et al., 2014; Wang et al., 2018). Regeneration from callus is less efficient in plants deprived of HIRA, whereas CAF-1 mutants are more efficient (Nie et al., 2014). Hence, selective incorporation and dynamic exchange of specific histone 3 variants might be an important mechanism underlying cell fate reprogramming during regeneration.

In addition to the H3 variants present in all multicellular eukaryotes, further H3 variants have been reported in *Arabidopsis* (Jiang and Berger, 2017b), including H3.10, which is expressed specifically in sperm (Okada et al., 2005; Borg and Berger, 2015), and H3.14, which is expressed in the vegetative pollen cell and in endosperm (Ingouff et al., 2010). With the exception of H3.10 (Borg et al., 2020), the properties and role of other atypical

[1]Natural Sciences and Science Education, National Institute of Education, Nanyang Technological University, 1 Nanyang Walk, Singapore 637616, Singapore. [2]Gregor Mendel Institute, Austrian Academy of Sciences, Vienna BioCenter, Dr. Bohr-Gasse 3, 1030 Vienna, Austria.

*Author for correspondence (zhong.chen@nie.edu.sg)

Z.C., 0000-0003-1632-1389

Handling Editor: Ykä Helariutta
Received 18 September 2019; Accepted 28 April 2020

Development (2020) 147, dev184895. doi:10.1242/dev.184895

Arabidopsis histone variants have not yet been elucidated. Here, we report that the histone 3 variant H3.15, which is encoded by the gene *HTR15* (Talbert et al., 2012), is involved in cell fate reprogramming during plant regeneration in *Arabidopsis*. H3.15 rapidly accumulates upon wounding and promotes callus development. H3.15 lacks residue K27 and consequently impacts H3K27me3 dynamics at genes important for regeneration. Our study suggests a new mechanism for the removal of PRC2-mediated gene repression during plant regeneration.

RESULTS

H3.15 is induced at wound sites

To analyze histone 3 variant dynamics during wound-induced regeneration, we analyzed gene expression in response to injury of hypocotyls and roots. We checked all H3 encoding (HTR) genes except *HTR7* and *HTR11*, which might be pseudogenes (Okada et al., 2005; Ingouff et al., 2010), and *HTR10*, which is specifically expressed in sperm (Okada et al., 2005; Borg and Berger, 2015). Quantitative RT-PCR (qRT-PCR) analysis showed that, among the 12 genes encoding H3 variants, the expression of *HTR15* (At5g12910) gradually increased upon wounding, in contrast with other H3 variants coding genes (Fig. 1A,B). We further tested the wound-induced expression of *HTR15* using GLUCURONIDASE (GUS) (Fig. S1A) or green fluorescent protein (GFP) reporter lines (Fig. 1C) under the control of the *HTR15* promoter. Confocal imaging indicated that GFP expression was detectable at wound sites of roots within 7 h (Fig. 1C) and in hypocotyls within 21 h of wounding (Fig. S1A). *HTR15* promoter activity was also detected at wound sites in other tissues, including roots and petioles (Fig. S1B-D). During wound-induced callus formation in roots, *pHTR15* first drove expression in the pericycle around the wound site (Fig. 1D-H) and later in proliferating callus cells (Fig. 1C; Fig. S1A). These observations indicate that the expression of *HTR15* is induced upon wounding and is sustained during callus formation.

HTR15 is expressed during auxin-induced callus formation

Explants incubated on auxin-rich CIM can form a callus from pericycle cells or pericycle-like cells (Ikeuchi et al., 2013). As *HTR15* is expressed in pericycle cells upon wounding, we tested whether *HTR15* expression is induced during CIM-induced callus formation. Time-course gene expression analysis using root explants indicated that *HTR15* expression was progressively induced during incubation on CIM (Fig. 2A). We further performed confocal imaging and GUS staining using *HTR15* reporter lines. *pHTR15* activity was strongly induced in the pericycle or pericycle-like cells of root and hypocotyl explants during CIM incubation (Fig. 2B; Fig. S2). These results

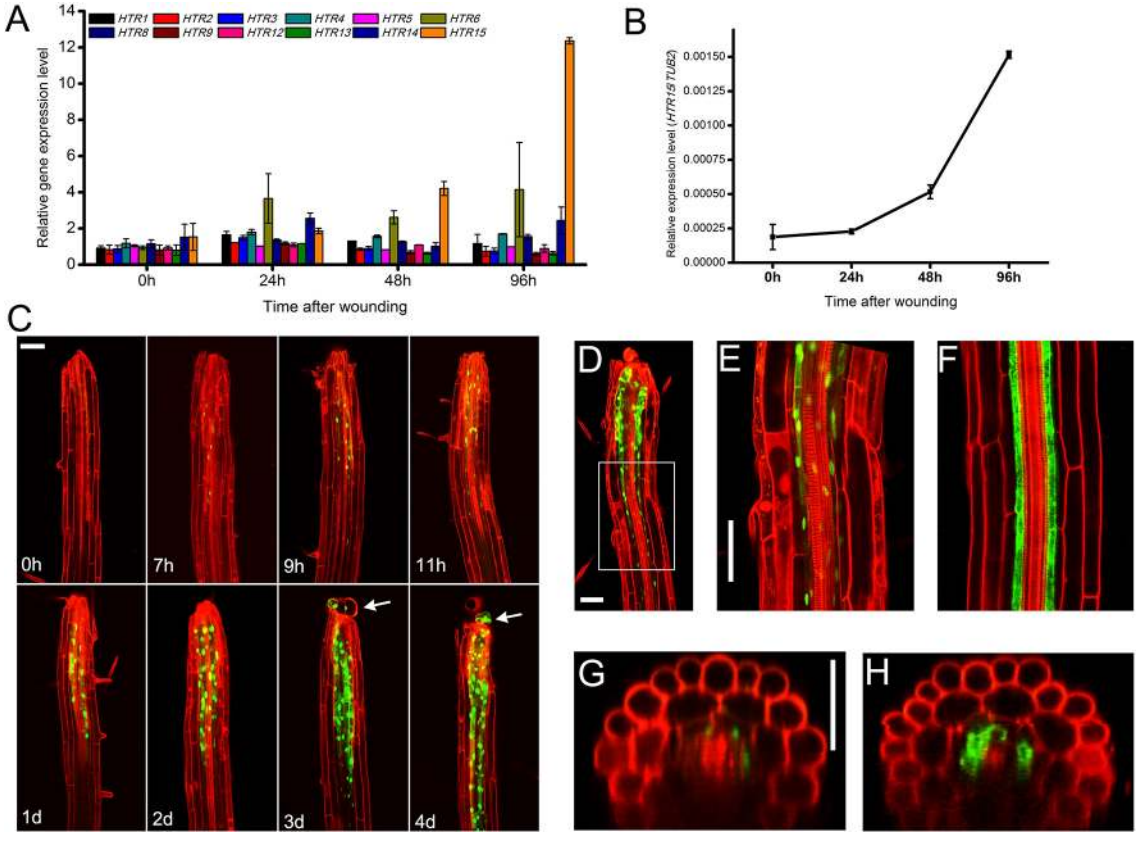

Fig. 1. *HTR15* expression is induced at wound sites in *Arabidopsis*. (A) qRT-PCR analysis shows the response of 12 HTRs to wounding. Seedlings (7 days old) were cut at the middle of hypocotyl; the upper parts were removed and the lower parts were incubated on phytohormone-free MS medium. Wounding tissues about 1 mm in length at the cutting site were collected for RNA extraction at indicated timepoints. Data are mean±s.d. (n=3 biological replicates). (B) qRT-PCR analysis of *HTR15* expression at the wound site of *Arabidopsis* hypocotyl. (C) Confocal imaging showing accumulation of *pHTR15::3GFP* at wound sites of root at different timepoints after wounding. The roots of 7-day-old seedlings were cut at ∼2 cm (elongation zone) from the root-hypocotyl junction. The upper ends of seedlings were removed and remaining roots were subjected to confocal imaging. Cell boundaries are stained by propidium iodide. At least 20 seedlings were checked at each timepoint. Arrows indicate callus cells outside the original root-hypocotyl region. (D-H) Confocal sections show *HTR15* promoter activity in the pericycle around wound sites 24 h after wounding (D,E,G). The pericycle marker J0121 was used as a reference (F,H). Cross-sections were generated from confocal *z* stacks. Scale bars: 50 µm.

Development (2020) 147, dev184895. doi:10.1242/dev.184895

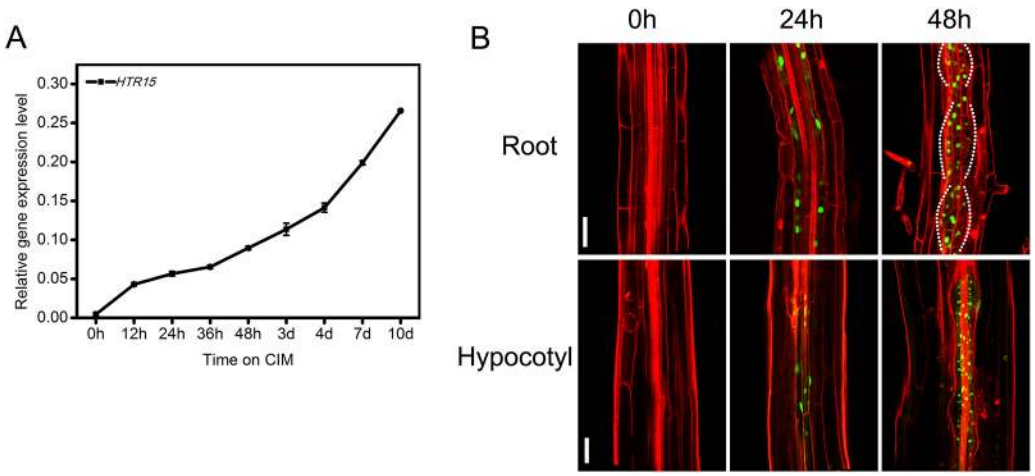

Fig. 2. *HTR15* expression is induced during CIM-induced callus formation. (A) qRT-PCR showing induction of *HTR15* expression when root explants are incubated on CIM. Data are mean±s.d. (*n*=3 biological replicates). (B) Confocal imaging shows *HTR15* promoter activity in the pericycle and pericycle-like cells. Root or hypocotyl explants of 7 days-old *pHTR15::3GFP* were incubated on CIM and confocal imaging was performed at the indicated timepoints. The area of *HTR15* promoter activity was outlined by white dotted lines in the upper right panel. Scale bars: 50 µm.

strongly suggest that *HTR15* expression is induced by auxin-rich CIM and sustained during CIM-induced callus formation.

Auxin is involved in the transcriptional control of *HTR15* during callus formation

Given that the plant hormone auxin is crucial for callus induction (Ikeuchi et al., 2013), we tested the impact of auxin on *HTR15* expression during wound-induced callus formation. *HTR15* expression was strongly induced by the synthetic auxin 1-naphthaleneacetic acid in lateral root primordium (Fig. S3) and whole seedlings (Fig. S4A), suggesting that *HTR15* expression is auxin inducible. Accordingly, the application of the auxin transport inhibitor 1-naphthylphthalamic acid delayed and reduced *HTR15* expression at wound sites (Fig. S4B), further suggesting a role for auxin in wound-triggered *HTR15* expression. Consistently, we found an auxin-responsive element (AuxRE, core sequence TGTCTC) located upstream of the *HTR15*-coding sequence (Fig. S4C). To test whether this motif controls wound-induced *HTR15* expression, we mutated AuxRE in the full-length *HTR15* promoter (*pHTR15-mAuxRE:GUS*). GUS staining revealed that this mutation delayed and impaired promoter activity upon wounding (Fig. S4B), suggesting that this AuxRE partially mediated *HTR15* induction in response to wounding. In addition, *pHTR15::3GFP* expression was much higher at wound sites than unwounded sites in root explants incubated on CIM (Fig. S4D). Altogether, these results indicate that *HTR15* transcription is mediated both by wounding and auxin during callus formation.

H3.15 promotes wound and auxin-induced callus formation

As pericycle cells possess pluripotency to develop into a callus (Atta et al., 2009; Sugimoto et al., 2010), the accumulation of H3.15 within the pericycle suggested that this H3 variant is involved in callus formation. To test the requirement of H3.15 in this process, we created an *htr15* knockout mutant using CRISPR/Cas9 technology. The mutated sequence contained a thymine (T) insertion at the 5′ end of the *HTR15*-coding sequence, creating a frameshift mutation that resulted in multiple premature stop codons (Fig. S5A). The null *htr15* allele produced smaller callus than wild type (Fig. 3A,B). This defect was complemented by introducing *pHTR15::HTR15* in *htr15* (Fig. S5B). To test whether H3.15 could enhance callus formation, we obtained transgenic plants overexpressing *HTR15* by fusing full-length genomic DNA to the cauliflower mosaic virus 35S promoter (*p35S::HTR15*) (Fig. S5C). Overexpression of *HTR15* produced significantly larger callus at hypocotyl wound sites compared with wild type (Fig. 3A,B). We further examined whether H3.15 was involved in CIM-induced callus formation. The root or hypocotyl explants were incubated on CIM for 40 days or 28 days, respectively, due to their tissue-specific differences in regeneration. We found that lines overexpressing *HTR15* had stronger callus-forming capacity than wild type in both CIM-cultured hypocotyl and root explants, whereas *htr15* explants produced significantly smaller callus (Fig. 3C-F). Moreover, complementation of *htr15* with *pHTR15::HTR15* fully restored callus-forming capacity (Fig. S5D). We therefore conclude that H3.15 plays an important role in promoting wound- and CIM-induced callus formation.

H3.15 reduces H3K27me3 levels during callus formation

Because histone H3 variants are variable at some specific amino acid residues, which are crucial for their function, we carefully analyzed the amino acid composition of H3.15. Four amino acid substitutions at positions 31, 41, 87 and 90 discriminate H3.3 from H3.1 in *Arabidopsis* (Okada et al., 2005; Ingouff and Berger, 2010). Among the four key amino acid residues at positions 31, 41, 87 and 90, only Phe41 (Y41) is conserved in both H3.3 and H3.15, whereas the other three residues vary among H3.1, H3.3 and H3.15 (Fig. 4A). Y41 was shown to be dispensable for the proper deposition of H3.3 (Lu et al., 2018), whereas alanine-31 (A31) in H3.1 is responsible for selective K27 monomethylation by the plant-specific Set domain histone methyltransferases ATXR5/6 (Jacob et al., 2014). The residues at positions 87 and 90 are crucial for interaction with the CAF-1 and HIRA complexes that deposit H3.1 and H3.3, respectively (Shi et al., 2011; Lu et al., 2018). In H3.15, these residues are substituted with residues that are present in neither H3.1 nor H3.3, preventing the prediction of the mechanisms involved in the deposition of H3.15 (Fig. 4A). In addition, *HTR15* lacks introns similar to H3.1-encoding genes, whereas H3.3-encoding genes contain introns within the coding sequence. To investigate whether H3.15 deposition is DNA replication-dependent in common with H3.1, we performed EdU

Development (2020) 147, dev184895. doi:10.1242/dev.184895

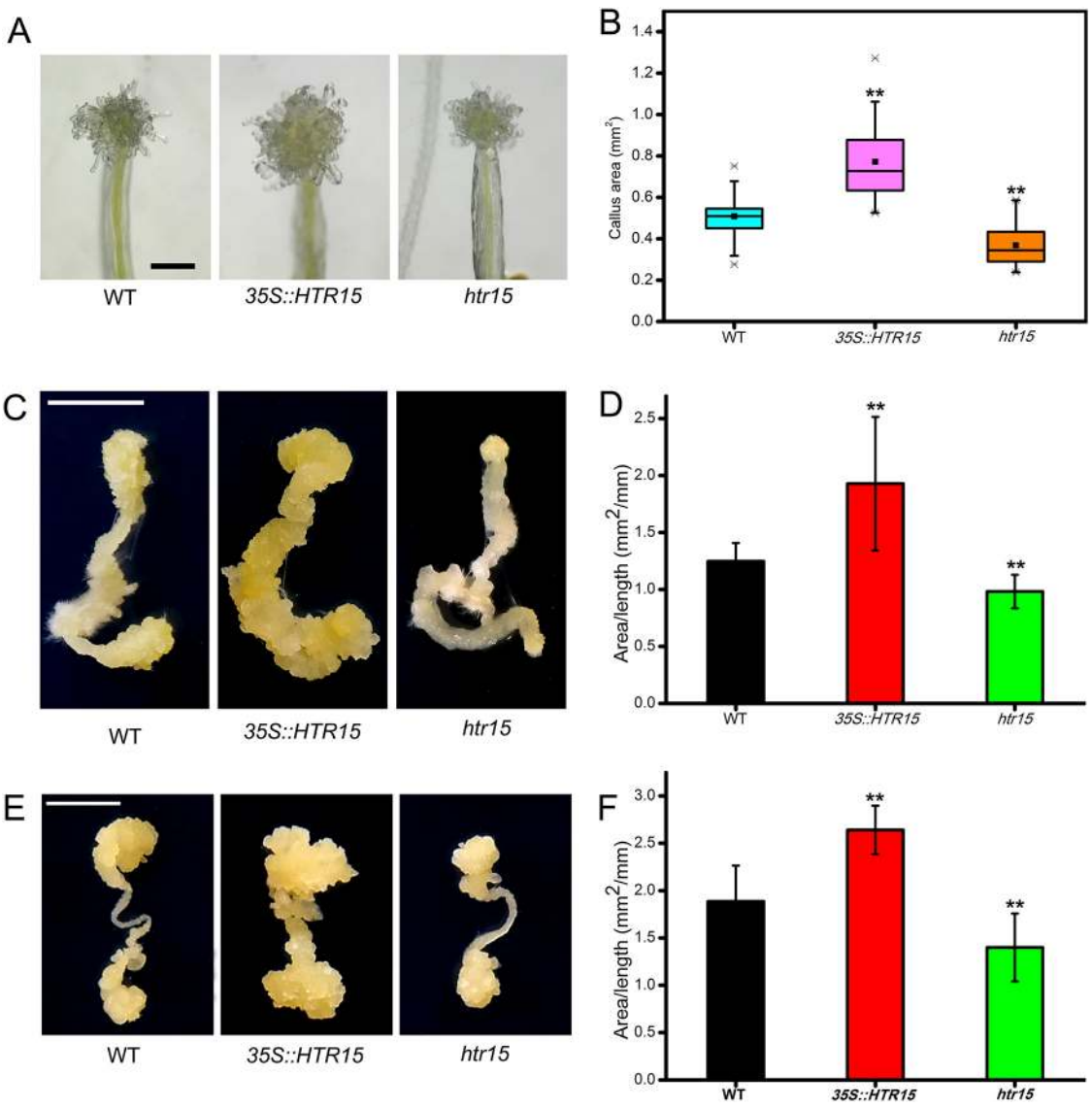

Fig. 3. H3.15 is required for wound-induced and auxin-induced callus formation. (A) Callus formed at wound site of wild-type, *35S::HTR15* and *htr15* hypocotyls 14 days after wounding. (B) Quantitative analysis of callus formation at wound sites of wild-type, *35S::HTR15* and *htr15* hypocotyls. After dissection, explants were cultured on phytohormone-free MS medium for 14 days. Box plots represent the distribution of projected callus area (n>28). The horizontal line in the box represents the median, the lower and upper boundaries of the box represent the lower (25%) and upper (75%) quartiles of the data, and the whiskers represent the minimum and maximum values. The statistical significance was determined by a two-tailed unpaired Student's t-test (**P<0.01). (C,D) CIM-induced callus formation of wild-type, *35S::HTR15* and *htr15* hypocotyl explants. The hypocotyl explants were incubated on CIM for 28 days. The length and area of hypocotyl explants were measured with Image-Pro plus 6.0 software. Data are mean±s.d. (n≥14; **P<0.01; two-tailed unpaired Student's t-test). (E,F) CIM-induced callus formation of wild-type, *35S::HTR15* and *htr15* root explants. The root explants were incubated on CIM for 40 days. Data are mean±s.d. (n≥12; **P<0.01; two-tailed unpaired Student's t-test). Scale bars: 0.5 mm (A); 5 mm (C,E).

staining and GUS staining assays to compare the wound-induced expression of *HTR15* with DNA replication. As shown in Fig. S6, DNA replication took place 24 h after wounding (Fig. S6A), whereas *CYCLIN B1;1* promoter activity was detected 48 h after wounding (Fig. S6B), much later than when *HTR15* expression was induced (Fig. 1C), suggesting that H3.15 transcription is activated prior to DNA replication, and H3.15 deposition is possibly not coupled with DNA replication but rather depends on the replication-independent chaperone HIRA, which has also been shown to promote callus formation (Nie et al., 2014). The substitutions in positions 87 and 90 led us to postulate that H3.15 might be deposited less efficiently than H3.3 through interaction with HIRA.

Compared with other *Arabidopsis* H3 variants, H3.15 shows the lowest degree of homology and lacks K4 (Lys^4) and K27 (Lys^{27}) residues (Fig. 4A). K4 methylation is associated with transcriptional activity in eukaryotes, so we tested whether this substitution had an impact on the phenotype observed in *htr15* plants. Introducing *pHTR15:HTR15-N4K* in *htr15* mutants complemented the *htr15* phenotype (Fig. S5B,D), suggesting that defective methylation at K4 is not related to the impact of H3.15 on callus induction. We identified homologs of H3.15 in close relatives of *Arabidopsis thaliana*, *Arabis lyrata*, *Arabis halleri* and *Boechera stricta*, and observed that they shared numerous nearly identical substitutions in the region 17-42 of H3.3 and also in the SHAVLAL motif of H3.3 that is involved in the deposition by HIRA (Fig. S7). This contrasted with homologs of the

Development (2020) 147, dev184895. doi:10.1242/dev.184895

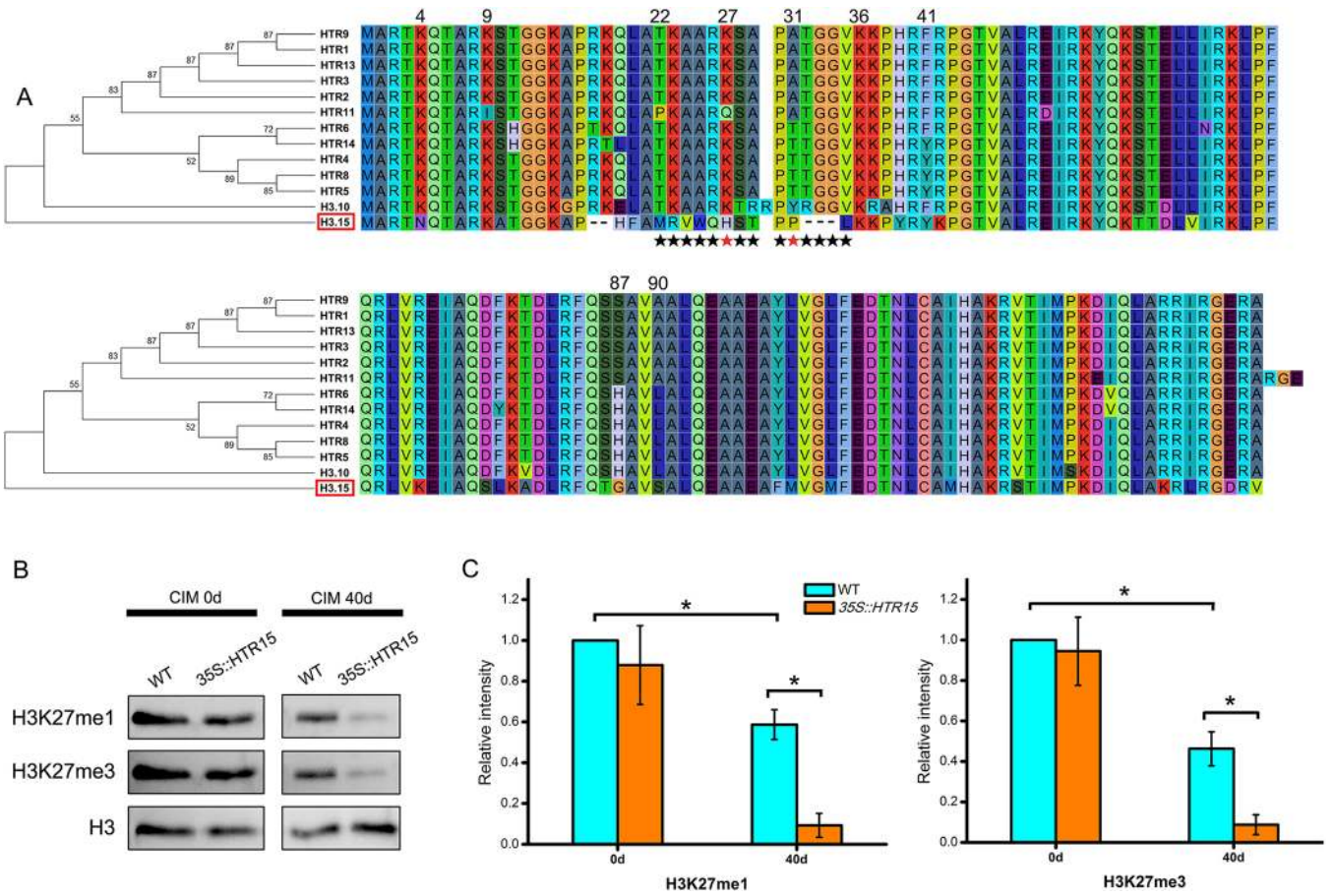

Fig. 4. H3.15 function is associated with H3K27me3. (A) Phylogenetic analysis and sequence alignment of H3 variants in *Arabidopsis* (excluding the centromeric H3 variant). (B) Western blot assay of H3K27me1 and H3K27me3 levels in non-callus tissue and CIM-induced callus. Wild-type and *35S::HTR15* hypocotyl explants were incubated on CIM for 40 days. H3 served as a loading control. (C) Quantification of H3K27me1 and H3K27me3 western blot signals in non-callus tissue and CIM-induced callus. The relative intensity of H3K27me1 and H3K27me3 were calculated by normalizing the signal to the loading control and then by normalizing the value for *35S::HTR15* against that for the wild type. The value of wild type at day 0 was set as 1. Data are mean±s.d. (n=3 biological replicates). *P<0.05; two-tailed unpaired Student's t-test.

other most divergent variant H3.10, which harbors K27 but lacks the proper residues in positions 28-32. We also identified likely homologs of H3.10 and H3.15 in more distantly related species of Brassicaceae, *Brassica oleracea*, *Capsella rubella* and *Capsella grandiflora*, as well as in *Medicago truncatula*. The degree of homology between the sequences of these proteins supports the idea that H3.15 and H3.10 represent two classes of divergent H3 variants that evolved in dicots. These variants probably play distinct roles because homologs of H3.10 carry the residue K27 and in *Arabidopsis* this variant is expressed specifically in sperm to reprogram H3K27me3 (Okada et al., 2005; Borg and Berger, 2015; Borg et al., 2020), whereas H3.15 is induced by wounding and callus induction, and is distinguished by the absence of K27.

We thus hypothesized that H3.15 incorporation could result in a loss of H3K27 methylation during callus formation. We performed immunoblotting analysis of *35S::HTR15* and wild type to examine H3K27 methylation levels. *35S::HTR15* showed levels of H3K27me1 and H3K27me3 similar to wild type before CIM induction (Fig. 4B,C). This suggested that ectopically expressed H3.15 is not incorporated in the absence of callus induction by CIM application. However, 40 days after CIM incubation, CIM-induced callus of *35S::HTR15* lines showed a dramatic reduction in both H3K27me1 and H3K27me3 levels compared with wild type (Fig. 4B,C). Hence, specifically during CIM-induced callus formation, overexpression of H3.15 globally reduces H3K27me1 and H3K27me3 levels compared with wild type.

To further test whether H3.15 function is correlated with the modification of K27, we introduced K27 in place of H3.15 H27 (His^{27}) (Fig. 5A) and overexpressed this mutant version in transgenic plants. Interestingly, H27K substitution did not block the effect of H3.15 on callus formation, as *35S::HTR15-H27K* still showed higher callus-forming capacity than wild type (Fig. 5B,C). We hypothesised that this was because of several other amino acid residues being substituted around K27 in H3.15 compared with wild type (Fig. 5A). A31 (Ala^{31}) is crucial for selective monomethylation of H3 at K27 (Jacob et al., 2014; Jiang and Berger, 2017a), whereas residues 28 and 29 are crucial for trimethylation by PRC2 (Moritz and Trievel, 2018). We thus made further substitutions and inserted residues between 22 and 35 to restore an amino acid sequence identical to that of H3.1 (Fig. 5A). Transgenic plants overexpressing this mutated form of *HTR15* (*35S::HTR15-KA*) showed a similar phenotype to wild type (Fig. 5B,C), showing that this mutated H3.15 variant lost capacity to promote callus formation. These results suggest that the immunity of H3.15 to K27 trimethylation is responsible for promoting callus induction. Furthermore, western blot assays revealed that H3K27me1 and H3K27me3 levels were lower in *35S::HTR15-H27K* than in wild type, whereas *35S::HTR15-KA* showed similar H3K27me3 levels as wild type

Development (2020) 147, dev184895. doi:10.1242/dev.184895

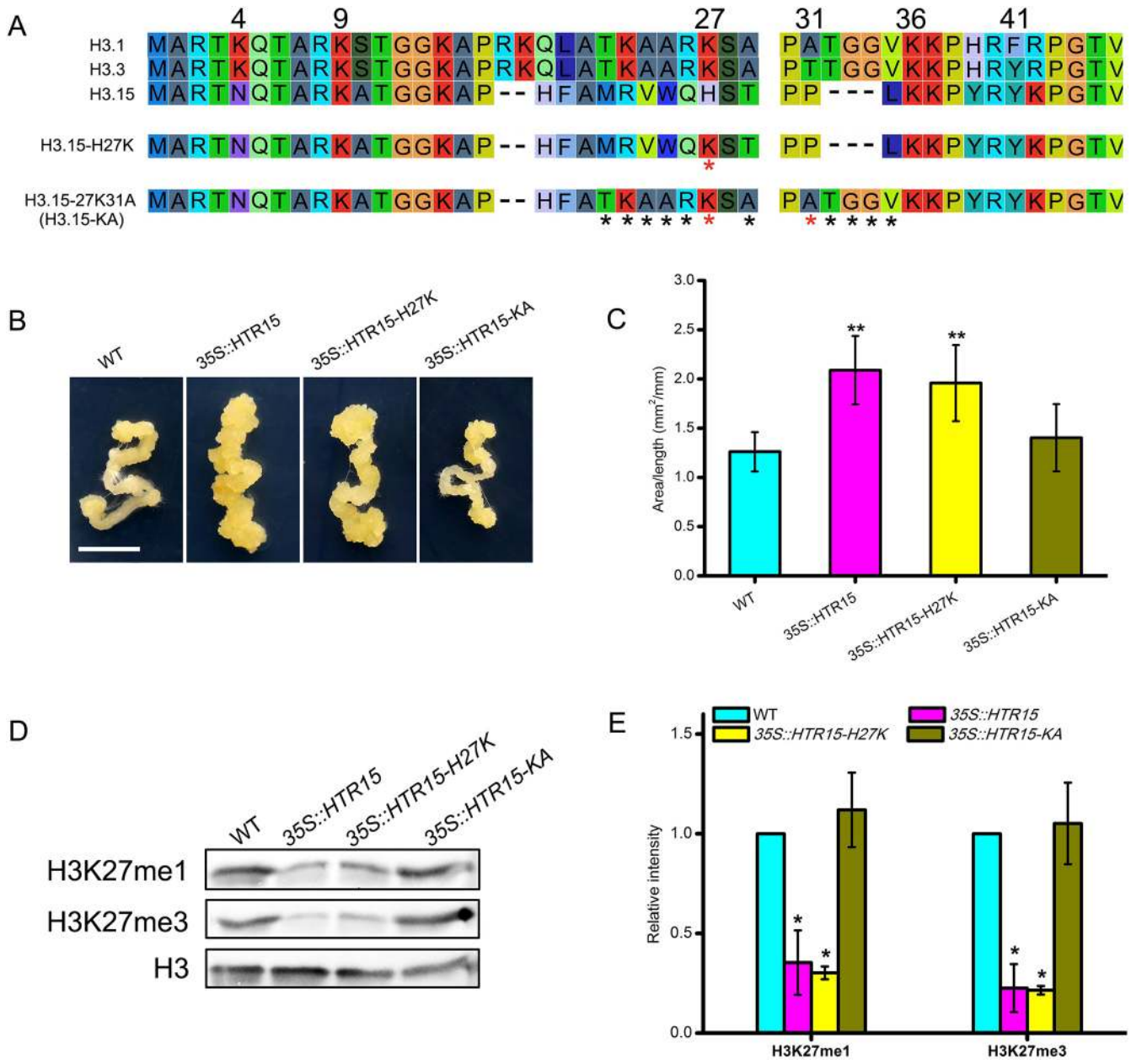

Fig. 5. Amino acid substitution analysis of H3.15. (A) Amino acid substitution of H3.15. (B) CIM-induced callus formation in wild type, *35S::HTR15*, *35S::HTR15-H27K* and 35S*::HTR15-KA*. The hypocotyl explants were incubated on CIM for 28 days. Scale bar: 5 mm. (C) Quantitative analysis of callus formation in wild-type, *35S::HTR15*, *35S::HTR15-H27K* and 35S*::HTR15-KA* hypocotyl explants. Data are mean±s.d. ($n \geq 10$; ***P*<0.01; two-tailed unpaired Student's *t*-test). (D) Western blot assay of H3K27me1 and H3K27me3 levels in CIM-induced callus. Wild-type, *35S::HTR15*, *35S::HTR15-H27K* and 35S*::HTR15-KA* hypocotyl explants were incubated on CIM for 30 days. H3 served as a loading control. (E) Quantification of H3K27me1 and H3K27me3 western blot signals in CIM-induced callus. *y*-axis values are fold changes of signals in transgenic lines compared with wild type. Data are mean±s.d. (n=3 biological replicates). **P*<0.05; two-tailed unpaired Student's *t*-test.

(Fig. 5D,E), indicating that the amino acid residues surrounding K27 affected H3K27me3 accumulation. Altogether, these results demonstrate that the function of H3.15 is strongly linked with the dynamics of histone methylation at K27.

H3.15 acts upstream of WOX11 and LBD18 to promote CIM-induced callus formation

To further understand how H3.15 regulates cell dedifferentiation and proliferation during callus formation, we examined the expression of key callus-forming regulators, including WOX11, LATERAL ORGAN BOUNDARIES-DOMAIN (LBDs) and ETHYLENE RESPONSE FACTOR 115 (ERF115) in CIM-cultured hypocotyl explants of wild type and *35S::HTR15*. *WOX11*, *LBD16*, *LBD18*, *LBD29* and *ERF115* expression was enhanced in *35S::HTR15* compared with wild type (Fig. 6A), suggesting that overexpression of H3.15 promotes transcription of these regulators during callus induction.

We further tested whether H3.15 was deposited in chromatin at the *WOX11* and *LBD18* locus. We produced plants overexpressing the fusion of H3.15 with 3×FLAG (Fig. S8). We performed ChIP assays with transgenic *35S::HTR15-3×FLAG* hypocotyl explants cultured on CIM for 30 days. The relative enrichment of H3.15 was

Development (2020) 147, dev184895. doi:10.1242/dev.184895

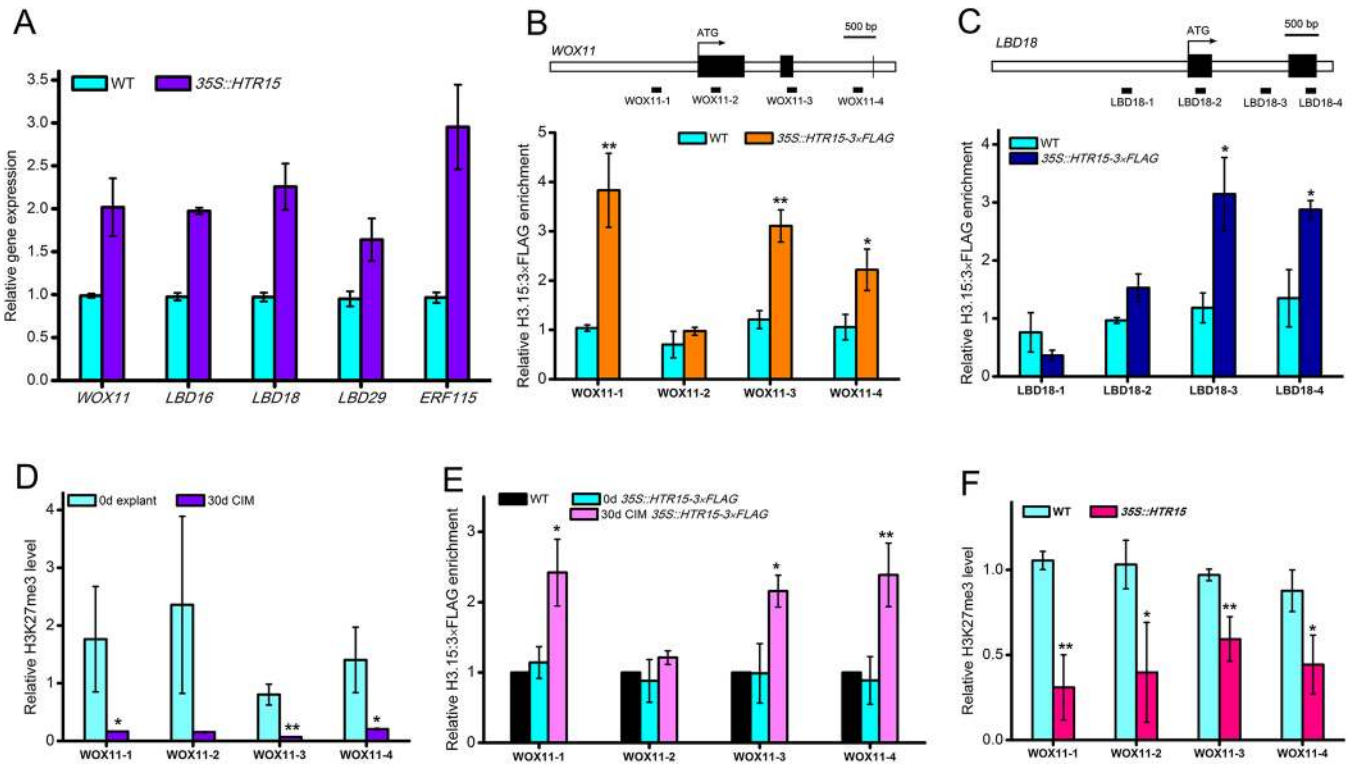

Fig. 6. H3.15 acts upstream of regeneration regulators to promote callus formation. (A) qRT-PCR analysis of regeneration regulators in wild-type and *35S::HTR15* hypocotyl explants cultured on CIM. Total RNA was extracted from hypocotyl explants cultured on CIM for 8 days. Data are mean±s.d. (*n*=3 biological replicates). (B) ChIP-qPCR analysis of H3.15 enrichment at *WOX11* locus. Hypocotyl explants cultured on CIM for 30 days were harvested. A schematic of the *WOX11* gene structure is shown above the panel. Black boxes represent exons and white boxes indicate intergenic regions and introns. Black boxes below the gene structure indicate regions examined by ChIP-qPCR. (C) ChIP-qPCR analysis of H3.15 enrichment at the *LBD18* locus. Hypocotyl explants cultured on CIM for 30 days were harvested. The relative enrichment of H3.15 was quantified by normalizing the amount of immunoprecipitated fragment to input DNA and then by normalizing the value for *35S::HTR15-3×FLAG* against the value for the wild type as a negative control. A schematic of the *LBD18* gene structure is shown above the panel. (D) ChIP-qPCR analysis of H3K27me3 accumulation at the *WOX11* locus during callus formation in wild type. Hypocotyl explants were harvested at day 0 or 30 days after cultured on CIM. The relative enrichment of H3K27me3 on the *WOX11* chromatin was calculated by normalizing the amount of immunoprecipitated fragment to input DNA and then by normalizing the value for the 30 days CIM sample against that for day 0 explants. (E) ChIP-qPCR analysis of H3.15 enrichment at *WOX11* locus during callus formation. The relative enrichment of H3.15 on the *WOX11* chromatin was calculated by normalizing the amount of immunoprecipitated fragment to input DNA and then by normalizing the value for 30 days CIM explants or day 0 explants of *35S::HTR15-3×FLAG* against that for wild type. The enrichment level in wild-type seedlings was set to 1. (F) ChIP-qPCR analysis of H3K27me3 levels at *WOX11* locus in wild type and *35S::HTR15*. Hypocotyl explants cultured on CIM for 30 days were harvested. The relative enrichment of H3K27me3 on the *WOX11* chromatin was calculated by normalizing the amount of immunoprecipitated fragment to input DNA and then by normalizing the value for *35S::HTR15* against that for the wild type. Data are mean±s.d. (*n*=3; **P*<0.05; ***P*<0.01; two-tailed unpaired Student's *t*-test).

quantified by normalizing the amount of immunoprecipitated fragment to input DNA, then to the enrichment of *35S::HTR15-3×FLAG* against wild type as a negative control. qPCR analysis showed that H3.15:3×FLAG was enriched on *WOX11* and *LBD18* chromatin both at the promoter and within the gene body (Fig. 6B,C). This indicated that H3.15 was incorporated in chromatin of *WOX11* and *LBD18* when overexpressed, which in turn likely impacted the levels of H3K27me3 at these loci.

A previous study profiled H3K27me3 dynamics during the leaf-to-callus transition in *Arabidopsis* (He et al., 2012). Using these data, we found that H3K27me3 levels at the *WOX11* and *LBD18* locus are reduced in the CIM-induced callus compared with non-callus leaf tissue (Fig. S9). Using ChIP-qPCR, we confirmed that enrichment of H3K27me3 at the *WOX11* locus was reduced during callus formation in the wild-type background (Fig. 6D). In plants expressing H3.15:3×FLAG under the control of the 35S promoter, H3.15 was not deposited at the *WOX11* locus in the absence of callus induction (Fig. 6E). However, enrichment of H3.15:3×FLAG was increased in the callus when compared with non-induced explants (Fig. 6E, day 0), suggesting that there is a negative correlation between H3.15 enrichment and H3K27me3 levels during callus formation. If H3.15 was directly involved in reducing H3K27me3 during callus formation, we would expect that overexpression of *HTR15* would reduce H3K27me3 enrichment at the *WOX11* locus further than in wild type in response to callus formation. We performed ChIP-qPCR for H3K27me3 at the *WOX11* locus in wild type and *35S::HTR15* explants after CIM incubation, and found that H3K27me3 levels were indeed lower in *35S::HTR15* than in wild type (Fig. 6F). Therefore, these results supported the notion that the deposition of H3.15 at the *WOX11* locus is triggered by callus formation, facilitates the removal of H3K27me3 at the *WOX11* locus and promotes expression of *WOX11* during callus formation. Consistently, a *pWOX11::GUS* reporter confirmed that *WOX11* promoter activity is higher in *35S::HTR15* than wild type during CIM incubation (Fig. S10). Previous studies showed that WOX11 promotes callus formation on leaf explants incubated on CIM (Liu et al., 2014), whereas ectopic expression of *LBD16*, *LBD17*, *LBD18* and *LBD29* resulted in spontaneous callus formation without exogenous phytohormone in *Arabidopsis* (Fan et al., 2012). Our results suggest that H3.15 promotes callus formation via the WOX11 and LBD-regulated

Development (2020) 147, dev184895. doi:10.1242/dev.184895

pathway by directly causing the removal of H3K27me3 and activating the expression of *WOX11* and *LBD* genes.

DISCUSSION

H3K27me3 is typically associated with gene repression (Kouzarides, 2007; Zhang et al., 2009; Roudier et al., 2011; Ikeuchi et al., 2015b). Under normal growth conditions, PRC2-mediated H3K27me3 maintains the differentiated states of mature somatic cells and prevents unscheduled cell dedifferentiation by repressing cell fate reprogramming regulators in *Arabidopsis* (Ikeuchi et al., 2015a). During plant regeneration, repression of cell dedifferentiation regulators by H3K27me3 is removed through H3K27 demethylation or other mechanisms that facilitate the activation of cell fate reprogramming and subsequent plant regeneration (Liu et al., 2014; Zhang et al., 2017). Hence, dynamic reprogramming of H3K27me3 is crucial for cell fate transition during plant regeneration. In this study, we reveal how the histone variant H3.15 promotes wound- and auxin-induced callus formation. Overexpression of *HTR15* enhanced the capacity to form callus, whereas its depletion compromised this response. Reporter analyses suggest that H3.15 accumulates in the root pericycle or pericycle-like cells of aerial organs, in which callus formation is initiated (Che et al., 2007; Atta et al., 2009; Sugimoto et al., 2010). H3.15 lacks the K27 residue that carries the repressive mark H3K27me3, and we have shown how H3.15 deposition correlates with a decrease of H3K27me3 in *HTR15* overexpression lines. Further studies are required to profile the global deposition of H3.15 and the mechanism that drives H3.15 replacement. Therefore, based on the data derived from *HTR15* overexpression lines, we propose that H3.15 deposition leads to the replacement of nucleosomes carrying H3K27me1 or H3K27me3 at specific loci by unmarked nucleosomes, resulting in the removal of these modifications and the reprogramming of downstream transcription.

Our study identified *WOX11* and *LBD18* as direct downstream targets of H3.15. WOX11 is required in the first step of cell fate transition from procambium cells to root founder cells during *de novo* root organogenesis. Overexpression of *WOX11* results in rapid callus formation on CIM (Liu et al., 2014). WOX11 functions in cooperation with LBD16 to promote pluripotency acquisition in callus cells (Liu et al., 2018). Previous studies showed that H3K27me3 levels at the *WOX11* locus are dramatically reduced during CIM-induced callus formation from leaf explants (He et al., 2012; Liu et al., 2014). As *WOX11* is activated by auxin in pericycle or procambium cells (pericycle-like cells) (Liu et al., 2014), which has a similar expression to *HTR15*, it is likely that H3.15 promotes *WOX11* expression in these cells. Observations of *HTR15* overexpression lines, supported the observation that H3.15 is enriched at *WOX11* chromatin during callus formation, thereby reducing H3K27me3 levels to de-repress *WOX11* expression.

In conclusion, we propose that H3.15 promotes local chromatin reprogramming of callus formation regulators to promote cell fate reprogramming required for callus formation (Fig. S11). As we have gathered evidence for H3.15 orthologs among dicots, similar mechanisms might work to mediate plant regeneration in other plant species; thus, our findings will probably extend to other species of flowering plants. The model reveals a mechanism whereby plant cells rapidly de-repress key meristem regulators and reprogram cell fate to reacquire pluripotency. In the moss *Physcomitrella*, regeneration involves H3K27me3-dependent trans-dedifferentiation of differentiated cells into stem cells without the generation of callus (Ishikawa et al., 2019). Bryophytes encode only CenH3, H3.1 and H3.3 variants (Bowman et al., 2017), and H3.15 probably evolved in flowering plants to facilitate the reprogramming of differentiated cells to initiate callus formation, which is required to regenerate new tissues after partial loss of tissue through injury. It will be of interest to investigate whether H3.15-like variants also contribute to developmentally programmed regeneration and whether H3.15 variants could be harnessed to improve plant cloning for biotechnological purposes.

MATERIALS AND METHODS

Plant materials

All *Arabidopsis* plants used in this study were in the Col-0 background. The reporter line J0121 was described previously (Laplaze et al., 2005). *Arabidopsis* seeds were sterilized with 75% ethanol and 15% bleach, and germinated on half-strength Murashige and Skoog (MS) plates [2.21 g/l MS basal medium with vitamin powder, 0.5 g/l 2-(N-morpholino) ethanesulfonic acid (MES), 10 g/l sucrose and 8 g/l agar (pH 5.7)]. Seven-day-old seedlings were transferred to soil and grown in a growth chamber at 22°C with a 16 h light and 8 h dark photoperiod.

Plasmid construction

For construction of *p35S::HTR15*, the *HTR15*-coding region was amplified from genomic DNA. After digestion, the fragment was inserted into pGIIK-p35S-LIC-NOSt (De Rybel et al., 2011). For generation of the *htr15* mutant, CRISPR/Cas9 technology was used as described previously (Wang et al., 2015). A pair of sgRNA targets (DT1, AGACAGCTCGTAAGGCAAC; DT2, AGATCAACTATCATGCCTA) in *HTR15* were selected and cloned into the pHEE401E vector. Then the CRISPR construct was transformed into the *Arabidopsis* Col-0 background via *Agrobacterium* strain GV3101. The homozygous *htr15* mutant was identified by DNA sequencing. For the complementation of *htr15*, a genomic fragment of *HTR15*, which included the promoter region and stop codon, was cloned into pGIIK-LIC-NOSt to obtain *pHTR15:HTR15*. This construct was transformed into the homozygous *htr15* mutant. To construct *pHTR15::GUS* and *pHTR15::3GFP*, the 1952 bp genomic fragment upstream of the *HTR15*-coding region was cloned into pGIIK-LIC-GUS-NOSt and pGIIK-LIC-SV40-3×GFP-NOSt, respectively. To generate the *p35S::HTR15-3×FLAG* construct, a genomic DNA fragment containing the full length of *HTR15* (without stop codon) was cloned into pGIIK-LIC-35S-3FLAG-NOSt. The HTR15-H27*K*, HTR15-N4*K* and HTR15-27K31A mutations were created by site-directed mutagenesis following a protocol described previously (Liu and Naismith, 2008). All binary vector constructs were introduced into *Agrobacterium* strain GV3101, containing the pGreen helper plasmid pSOUP, and transformed into *Arabidopsis* Col-0 using the floral dip method (Clough and Bent, 1998). Transgenic seedlings were first selected on MS agar plates with appropriate antibiotics and further confirmed by qRT-PCR, histochemical GUS assays or confocal imaging. Primers for plasmid construction are listed in Table S1.

Callus formation assay

After 3 days at 4°C in the dark, *Arabidopsis* seeds were germinated on half-strength MS plates [2.21 g/l MS basal medium with vitamin powder, 0.5 g/l MES, 10 g/l sucrose, and 8 g/l agar (pH 5.7)]. To induce callus formation by wounding, 7-day-old seedlings were dissected with microscissors at the middle of the hypocotyl (the upper end of hypocotyls and cotyledon were removed). Remaining seedlings were incubated on half-strength MS plates. To induce callus from root or hypocotyl explants, plant roots or etiolated hypocotyls were excised and transferred to auxin-rich CIM (3.21 g/l Gamborg B5 medium with vitamin powder, 20 g/l sucrose, 0.5 g/l MES, 8 g/l phytoagar and 2.2 µM 2,4-D, 0.2 µM kinetin) and incubated at 22°C under long-day conditions. Three independent experiments were performed.

Gene expression analysis

Total RNA was isolated from *Arabidopsis* hypocotyls at wound sites or from callus, induced by CIM, using NucleoSpin RNA Plant Mini Kit (Macherey-Nagel) following the manufacturer's instructions. cDNA was synthesized using the cDNA synthesis Kit (Thermo Scientific, K1639) from 2 µg of total

RNA in a 20 µl reaction. qRT-PCR was performed on an ABI StepOnePlus Real-Time PCR System (Life Technologies) using SYBR green (KAPA SYBR Fast qPCR Kit) according to the manufacturer's instructions. Relative expression levels were calculated using the ΔΔCt (cycle threshold) method, and *PP2AA3* was used as an endogenous reference gene. Three biological replicates with two technical replicates were performed. Primers for qRT-PCR are listed in Table S1.

GUS staining

Tissues were prefixed in 90% acetone on ice for 20 min and incubated in GUS staining buffer [50 mM sodium phosphate (pH 7.0), 10 mM EDTA, 1 mg/ml 5-bromo-4-chloro-3-indoyl β-D-glucuronide, 0.5 mM potassium ferricyanide, and 0.5 mM potassium ferrocyanide, 0.1% (v/v) Triton X-100] at 37°C for 2 h. Stained samples were then cleared of chlorophyll in an ethanol series (35%, 50%, 75% and 90%) followed by clearing in chloral hydrate for several hours and then photographed using a light microscope.

Confocal imaging

Samples were first stained with 5 µg/ml of propidium iodide and then rinsed in water to remove excess propidium iodide before slide mounting. All images were taken with a Nikon A1R Laser Scanning Confocal Microscope. For GFP detection, a 488 nm laser was used for excitation and emission light wavelength was 510 to 550 nm; for propidium iodide detection, excitation light wavelength was 561 nm and emission was 631 to 690 nm.

EdU staining

After cutting, the roots of 7-day-old Col-0 seedlings were transferred onto half-strength MS medium supplemented with 10 µM EdU (Click-iT EdU Imaging Kit, Invitrogen). The roots were then fixed at different time points in 3.7% (v/v) formaldehyde with 1% (v/v) Triton-X 100 in 1×PBS solution for 30 min. EdU staining was performed with the Click-iT EdU Alexa Fluor 647 Imaging Kit following the manufacturer's instructions. Nuclei were labeled with Hoechst 33342 stain. The samples were imaged using a Nikon A1R Laser Scanning Confocal Microscope. For the detection of EdU staining, the excitation wavelength of 638 nm was used and emission wavelengths between 663 and 738 nm were collected. For the detection of Hoechst 333 staining, a 405 nm laser was used for excitation and emission light wavelength between 425 and 475 nm was collected.

Western blot

The extraction and purification of histones from plants has been described previously (Yan et al., 2007; Mahrez et al., 2016). Briefly, ∼100 mg of root explants were homogenized in histone extraction buffer [0.25 M sucrose, 1 mM $CaCl_2$, 15 mM NaCl, 60 mM KCl, 5 mM $MgCl_2$, 15 mM PIPES (pH 7.0), 0.5% Triton X-100, 10 mM sodium butyrate and a protease inhibitor cocktail]. After centrifugation for 20 min at 10,000 ***g***, pellets were resuspended with 0.2 M H_2SO_4 and incubated overnight at 4°C. After centrifugation for 10 min at 17,000 ***g***, total histones from the supernatant were precipitated with concentrated trichloroacetic acid to a final concentration of 33%. The histone pellet was washed twice with ice-cold acetone and air-dried for 20 min at room temperature. Pellets were then dissolved in double distilled water. All steps were carried out at 4°C or on ice, unless specified. Protein immunoblotting was performed with anti-H3 (Abcam, ab1791, 1:1000), anti-H3K27me1 (Millipore, 17-643, 1:1000) and anti-H3K27me3 (Millipore, 07-449, 1:1000) antibodies. The intensities of the protein bands were quantified by ImageJ and normalized to the loading control.

ChIP

ChIP assays were performed as described previously with modifications (Yamaguchi et al., 2014). Hypocotyl explants (300-500 mg) were fixed with 10 ml 1% formaldehyde solution under vacuum infiltration conditions. After adding glycine to a concentration of 125 mM to quench the crosslinker, the fixed samples were washed two times with ice-cold PBS solution and ground to a fine powder in liquid nitrogen. The resultant powder was resuspended in 2.5 ml of ice-cold PBS containing 25 µl of the Halt Cocktail and filtrated through Miracloth (Calbiochem). Nuclei collected by centrifugation were subjected to membrane extraction buffer containing protease/phosphatase inhibitors to lyse membrane and cytosol. The nuclei mixture was digested with micrococcal nuclease (Pierce Magnetic ChIP Kit, Thermo Scientific) and sonicated with an ultrasonic cell disruptor to break the nuclear membrane. An aliquot of solubilized chromatin (10%) was saved as an input control, and the remainder was incubated with anti-flag antibody (Abcam, ab1162, 1:80) or anti-H3K27me3 antibody (Millipore, 07-449, 1:80) for 2 h or overnight at 4°C with mixing. The Protein A/G magnetic beads were then added to the chromatin solution and collected using a magnetic stand after incubation for 2 h at 4°C with mixing. The beads were then collected and washed three times with IP Wash Buffer 1 and once with IP Wash Buffer 2. The washed beads were then incubated with the elution buffer for 40 min at 65°C. The eluted chromatin and the 10% input control were added with 5 M NaCl and 20 mg/ml Proteinase K, and incubated at 65°C for 2-6 h for reverse crosslinking. DNA was then recovered using a DNA clean-up column and reagents (Pierce Magnetic ChIP Kit, Thermo Scientific), and eluted in 50 µl of elution buffer. Purified DNA (1 µl) was subjected to qRT-PCR. Primer pairs used for the ChIP assays are listed in Table S1.

Acknowledgements

We thank the Nikon Imaging Centre at the Singapore Bioimaging Consortium for their assistance with confocal imaging.

Competing interests

The authors declare no competing or financial interests.

Author contributions

Conceptualization: F.B., Z.C.; Methodology: A.Y., M.B., Z.C.; Validation: A.Y., M.B.; Formal analysis: A.Y., F.B., Z.C.; Investigation: A.Y., Z.C.; Resources: F.B., Z.C.; Data curation: A.Y.; Writing - original draft: A.Y.; Writing - review & editing: F.B., Z.C.; Visualization: A.Y.; Supervision: Z.C.; Project administration: Z.C.; Funding acquisition: M.B., Z.C.

Funding

This work was supported by Nanyang Technological University (RI 8/16 CZ to A.Y. and Z.C.) and by the Austrian Science Fund (Liese Meitner M1818 to M.B.).

Supplementary information

Supplementary information available online at
http://dev.biologists.org/lookup/doi/10.1242/dev.184895.supplemental

Peer review history

The peer review history is available online at https://dev.biologists.org/lookup/doi/10.1242/dev.184895.reviewer-comments.pdf

References

Atta, R., Laurens, L., Boucheron-Dubuisson, E., Guivarc'h, A., Carnero, E., Giraudat-Pautot, V., Rech, P. and Chriqui, D. (2009). Pluripotency of Arabidopsis xylem pericycle underlies shoot regeneration from root and hypocotyl explants grown *in vitro*. *Plant J.* **57**, 626-644. doi:10.1111/j.1365-313X.2008.03715.x

Borg, M. and Berger, F. (2015). Chromatin remodelling during male gametophyte development. *Plant J.* **83**, 177-188. doi:10.1111/tpj.12856

Borg, M., Jacob, Y., Susaki, D., LeBlanc, C., Buendía, D., Axelsson, E., Kawashima, T., Voigt, P., Boavida, L., Becker, J. et al. (2020). Targeted reprogramming of H3K27me3 resets epigenetic memory in plant paternal chromatin. *Nat. Cell Biol.* [Epub ahead of print]. doi.org/10.1038/s41556-020-0515-y

Bowman, J. L. Kohchi, T. Yamato, K. T. Jenkins, J. Shu, S. Ishizaki, K. Yamaoka, S. Nishihama, R. Nakamura, Y. Berger, F. et al. (2017). Insights into land plant evolution garnered from the *Marchantia polymorpha* genome. *Cell* **171**, 287-304.e15. doi:10.1016/j.cell.2017.09.030

Che, P., Lall, S. and Howell, S. H. (2007). Developmental steps in acquiring competence for shoot development in Arabidopsis tissue culture. *Planta* **226**, 1183-1194. doi:10.1007/s00425-007-0565-4

Clough, S. J. and Bent, A. F. (1998). Floral dip: a simplified method for Agrobacterium-mediated transformation of *Arabidopsis thaliana*. *Plant J.* **16**, 735-743. doi:10.1046/j.1365-313x.1998.00343.x

De Rybel, B., van den Berg, W., Lokerse, A. S., Liao, C.-Y., van Mourik, H., Möller, B., Llavata-Peris, C. I. and Weijers, D. (2011). A versatile set of ligation-independent cloning vectors for functional studies in plants. *Plant Physiol.* **156**, 1292-1299. doi:10.1104/pp.111.177337

Fan, M., Xu, C., Xu, K. and Hu, Y. (2012). Lateral organ boundaries domain transcription factors direct callus formation in Arabidopsis regeneration. *Cell Res.* **22**, 1169-1180. doi:10.1038/cr.2012.63
He, C., Chen, X., Huang, H. and Xu, L. (2012). Reprogramming of H3K27me3 is critical for acquisition of pluripotency from cultured Arabidopsis tissues. *PLoS Genet.* **8**, e1002911. doi:10.1371/journal.pgen.1002911
Henikoff, S., Furuyama, T. and Ahmad, K. (2004). Histone variants, nucleosome assembly and epigenetic inheritance. *Trends Genet.* **20**, 320-326. doi:10.1016/j.tig.2004.05.004
Ikeuchi, M., Sugimoto, K. and Iwase, A. (2013). Plant callus: mechanisms of induction and repression. *Plant Cell* **25**, 3159-3173. doi:10.1105/tpc.113.116053
Ikeuchi, M., Iwase, A., Rymen, B., Harashima, H., Shibata, M., Ohnuma, M., Breuer, C., Morao, A. K., de Lucas, M., De Veylder, L. et al. (2015a). PRC2 represses dedifferentiation of mature somatic cells in Arabidopsis. *Nat. Plants* **1**, 15089. doi:10.1038/nplants.2015.89
Ikeuchi, M., Iwase, A. and Sugimoto, K. (2015b). Control of plant cell differentiation by histone modification and DNA methylation. *Curr. Opin. Plant Biol.* **28**, 60-67. doi:10.1016/j.pbi.2015.09.004
Ingouff, M. and Berger, F. (2010). Histone3 variants in plants. *Chromosoma* **119**, 27-33. doi:10.1007/s00412-009-0237-1
Ingouff, M., Rademacher, S., Holec, S., Šoljić, L., Xin, N., Readshaw, A., Foo, S. H., Lahouze, B., Sprunck, S. and Berger, F. (2010). Zygotic resetting of the HISTONE 3 variant repertoire participates in epigenetic reprogramming in Arabidopsis. *Curr. Biol.* **20**, 2137-2143. doi:10.1016/j.cub.2010.11.012
Ishikawa, M., Morishita, M., Higuchi, Y., Ichikawa, S., Ishikawa, T., Nishiyama, T., Kabeya, Y., Hiwatashi, Y., Kurata, T., Kubo, M. et al. (2019). Physcomitrella STEMIN transcription factor induces stem cell formation with epigenetic reprogramming. *Nat. Plants* **5**, 681-690. doi:10.1038/s41477-019-0464-2
Iwase, A., Mitsuda, N., Koyama, T., Hiratsu, K., Kojima, M., Arai, T., Inoue, Y., Seki, M., Sakakibara, H. Sugimoto, K. et al. (2011). The AP2/ERF transcription factor WIND1 controls cell dedifferentiation in Arabidopsis. *Curr. Biol.* **21**, 508-514. doi:10.1016/j.cub.2011.02.020
Iwase, A., Harashima, H., Ikeuchi, M., Rymen, B., Ohnuma, M., Komaki, S., Morohashi, K., Kurata, T., Nakata, M., Ohme-Takagi, M. et al. (2017). WIND1 promotes shoot regeneration through transcriptional activation of ENHANCER OF SHOOT REGENERATION1 in Arabidopsis. *Plant Cell* **29**, 54-69. doi:10.1105/tpc.16.00623
Jacob, Y., Bergamin, E., Donoghue, M. T., Mongeon, V., LeBlanc, C., Voigt, P., Underwood, C. J., Brunzelle, J. S., Michaels, S. D. Reinberg, D. et al. (2014). Selective methylation of histone H3 variant H3. 1 regulates heterochromatin replication. *Science* **343**, 1249-1253. doi:/10.1126/science.1248357
Jiang, D. and Berger, F. (2017a). DNA replication–coupled histone modification maintains Polycomb gene silencing in plants. *Science* **357**, 1146-1149. doi:10.1126/science.aan4965
Jiang, D. and Berger, F. (2017b). Histone variants in plant transcriptional regulation. *Biochim. Biophys. Acta Gene Regul. Mech.* **1860**, 123-130. doi:10.1016/j.bbagrm.2016.07.002
Kaya, H., Iwabuchi, M., Tabata, S., Sato, S., Araki, T. and Kobayashi, Y. (2000). hosoba toge, a syndrome caused by a large chromosomal deletion associated with a T-DNA insertion in Arabidopsis. *Plant Cell Physiol.* **41**, 1055-1066. doi:10.1093/pcp/pcd032
Kouzarides, T. (2007). Chromatin modifications and their function. *Cell* **128**, 693-705. doi:10.1016/j.cell.2007.02.005
Laplaze, L., Parizot, B., Baker, A., Ricaud, L., Martinière, A., Auguy, F., Franche, C., Nussaume, L., Bogusz, D. and Haseloff, J. (2005). GAL4-GFP enhancer trap lines for genetic manipulation of lateral root development in *Arabidopsis thaliana*. *J. Exp. Bot.* **56**, 2433-2442. doi:10.1093/jxb/eri236
Lee, K. and Seo, P. J. (2018). Dynamic epigenetic changes during plant regeneration. *Trends Plant Sci.* **23**, 235-247. doi:10.1016/j.tplants.2017.11.009
Liu, H. and Naismith, J. H. (2008). An efficient one-step site-directed deletion, insertion, single and multiple-site plasmid mutagenesis protocol. *BMC Biotechnol.* **8**, 91. doi:10.1186/1472-6750-8-91
Liu, J., Sheng, L., Xu, Y., Li, J., Yang, Z., Huang, H. and Xu, L. (2014). WOX11 and 12 are involved in the first-step cell fate transition during *de novo* root organogenesis in Arabidopsis. *Plant Cell* **26**, 1081-1093. doi:10.1105/tpc.114.122887
Liu, J., Hu, X., Qin, P., Prasad, K., Hu, Y. and Xu, L. (2018). The WOX11-LBD16 pathway promotes pluripotency acquisition in callus cells during de novo shoot regeneration in Arabidopsis tissue culture. *Plant Cell Physiol.* **59**, 739-748. doi:10.1093/pcp/pcy010
Loyola, A. and Almouzni, G. (2007). Marking histone H3 variants: how, when and why? *Trends Biochem. Sci.* **32**, 425-433. doi:10.1016/j.tibs.2007.08.004
Lu, L., Chen, X., Qian, S. and Zhong, X. (2018). The plant-specific histone residue Phe41 is important for genome-wide H3.1 distribution. *Nat. Commun.* **9**, 630. doi:10.1038/s41467-018-02976-9
Mahrez, W., Arellano, M. S. T., Moreno-Romero, J., Nakamura, M., Shu, H., Nanni, P., Köhler, C., Gruissem, W. and Hennig, L. (2016). H3K36ac is an evolutionary conserved plant histone modification that marks active genes. *Plant Physiol.* **170**, 1566-1577. doi:10.1104/pp.15.01744
Malik, H. S. and Henikoff, S. (2003). Phylogenomics of the nucleosome. *Nat. Struct. Biol.* **10**, 882-891. doi:10.1038/nsb996
Moritz, L. E. and Trievel, R. C. (2018). Structure, mechanism, and regulation of polycomb-repressive complex 2. *J. Biol. Chem.* **293**, 13805-13814. doi:10.1074/jbc.R117.800367
Nie, X., Wang, H., Li, J., Holec, S. and Berger, F. (2014). The HIRA complex that deposits the histone H3.3 is conserved in Arabidopsis and facilitates transcriptional dynamics. *Biol. Open* **3**, 794-802. doi:10.1242/bio.20148680
Okada, T., Endo, M., Singh, M. B. and Bhalla, P. L. (2005). Analysis of the histone H3 gene family in Arabidopsis and identification of the male-gamete-specific variant *AtMGH3*. *Plant J.* **44**, 557-568. doi:10.1111/j.1365-313X.2005.02554.x
Roudier, F., Ahmed, I., Bérard, C., Sarazin, A., Mary-Huard, T., Cortijo, S., Bouyer, D., Caillieux, E., Duvernois-Berthet, E., Al-Shikhley, L. et al. (2011). Integrative epigenomic mapping defines four main chromatin states in Arabidopsis. *EMBO J.* **30**, 1928-1938. doi:10.1038/emboj.2011.103
Shi, L., Wang, J., Hong, F., Spector, D. L. and Fang, Y. (2011). Four amino acids guide the assembly or disassembly of Arabidopsis histone H3.3-containing nucleosomes. *Proc. Natl. Acad. Sci. USA* **108**, 10574-10578. doi:10.1073/pnas.1017882108
Skoog, F. and Miller, C. O. (1957). Chemical regulation of growth and organ formation in plant tissues cultured in vitro. *Symp. Soc. Exp. Biol.* **11**, 118-130.
Sugimoto, K., Jiao, Y. and Meyerowitz, E. M. (2010). Arabidopsis regeneration from multiple tissues occurs via a root development pathway. *Dev. Cell* **18**, 463-471. doi:10.1016/j.devcel.2010.02.004
Sugimoto, K., Gordon, S. P. and Meyerowitz, E. M. (2011). Regeneration in plants and animals: dedifferentiation, transdifferentiation, or just differentiation? *Trends Cell Biol.* **21**, 212-218. doi:10.1016/j.tcb.2010.12.004
Talbert, P. B., Ahmad, K., Almouzni, G., Ausió, J., Berger, F., Bhalla, P. L., Bonner, W. M., Cande, W. Z., Chadwick, B. P., Chan, S. W. L. et al. (2012). A unified phylogeny-based nomenclature for histone variants. *Epigenetics Chromatin* **5**, 7. doi:10.1186/1756-8935-5-7
Wang, Z.-P., Xing, H.-L., Dong, L., Zhang, H.-Y., Han, C.-Y., Wang, X.-C. and Chen, Q.-J. (2015). Egg cell-specific promoter-controlled CRISPR/Cas9 efficiently generates homozygous mutants for multiple target genes in Arabidopsis in a single generation. *Genome Biol.* **16**, 144. doi:g/10.1186/s13059-015-0715-0
Wang, H., Jiang, D., Axelsson, E., Lorković, Z. J., Montgomery, S., Holec, S., Pieters, B. J. G. E., Al Temimi, A. H. K., Mecinović, J. and Berger, F. (2018). LHP1 interacts with ATRX through plant-specific domains at specific loci targeted by PRC2. *Mol. Plant* **11**, 1038-1052. doi:10.1016/j.molp.2018.05.004
Weber, C. M. and Henikoff, S. (2014). Histone variants: dynamic punctuation in transcription. *Gene Dev.* **28**, 672-682. doi:10.1101/gad.238873.114
Yamaguchi, N., Winter, C. M., Wu, M.-F., Kwon, C. S., William, D. A. and Wagner, D. (2014). Protocol: Chromatin immunoprecipitation from Arabidopsis tissues. *Arabidopsis Book* **12**, e0170. doi:10.1199/tab.0170
Yan, D., Zhang, Y., Niu, L., Yuan, Y. and Cao, X. (2007). Identification and characterization of two closely related histone H4 arginine 3 methyltransferases in *Arabidopsis thaliana*. *Biochem. J.* **408**, 113-121. doi:10.1042/BJ20070786
Zhang, X., Bernatavichute, Y. V., Cokus, S., Pellegrini, M. and Jacobsen, S. E. (2009). Genome-wide analysis of mono-, di- and trimethylation of histone H3 lysine 4 in *Arabidopsis thaliana*. *Genome Biol.* **10**, R62. doi:10.1186/gb-2009-10-6-r62
Zhang, T.-Q., Lian, H., Zhou, C.-M., Xu, L., Jiao, Y. and Wang, J.-W. (2017). A two-step model for *de novo* activation of WUSCHEL during plant shoot regeneration. *Plant Cell* **29**, 1073-1087. doi:10.1105/tpc.16.00863